IOP PUBLISHING JOURNAL OF PHYSICS: CONDENSED MATTER

J. Phys.: Condens. Matter **19** (2007) 395010 (9pp) doi:10.1088/0953-8984/19/39/395010

Ellipsometry and *ab initio* approaches to the refractive index of porous silicon

Rodolfo Cisneros, Carlos Ramírez and Chumin Wang[1]

Instituto de Investigaciones en Materiales, Universidad Nacional Autónoma de México, Apartado Postal 70-360, 04510, México DF, Mexico

E-mail: chumin@servidor.unam.mx

Received 13 February 2007, in final form 17 March 2007
Published 30 August 2007
Online at stacks.iop.org/JPhysCM/19/395010

Abstract

Spectroscopic ellipsometry is used to determine the complex refractive index ($n - ik$), porosity, and thickness of porous silicon (PSi) films. These films are obtained by anodizing p-type crystalline silicon in a hydrofluoric acid bath. After etching, PSi samples are heated to 750 °C in a controlled oxygen environment. A detailed analysis of the ellipsometry data is performed in order to determine the complex refractive index of PSi thin film. This frequency dependence of n and k is compared with the results of *ab initio* quantum mechanical calculations carried out by means of CASTEP codes within the density functional theory. The theoretical results show a diminution of the lattice constant as the oxygen content grows, in contrast to the hydrogen-saturated surface case.

(Some figures in this article are in colour only in the electronic version)

1. Introduction

Materials assembled by dots and wires on the nanometre scale have exceptional properties and broad applications. For example, they possess enhanced hardness, toughness, and catalytic capacity, as well as improved magnetic and optoelectronic properties, mainly caused by the quantum confinement of excitations and the large percentage of atoms at the surface [1]. In particular, porous silicon (PSi) has been a subject of enormous interest in the last 15 years, since nowadays microelectronics technology is essentially based on silicon, which is the second most abundant element on the earth's crust. PSi is usually sculpted by etching a crystalline silicon (c-Si) wafer in a solution of hydrofluoric acid. The resulting skeleton, shaped by interconnected Si nanowires, has a surface-to-volume ratio of 500 m^2 cm^{-3} and surprising optical properties. For example, PSi exhibits efficient photo- and electro-luminescence in the visible spectrum at room temperature [2], contrary to c-Si possessing an indirect band gap of 1.1 eV.

[1] Author to whom any correspondence should be addressed.

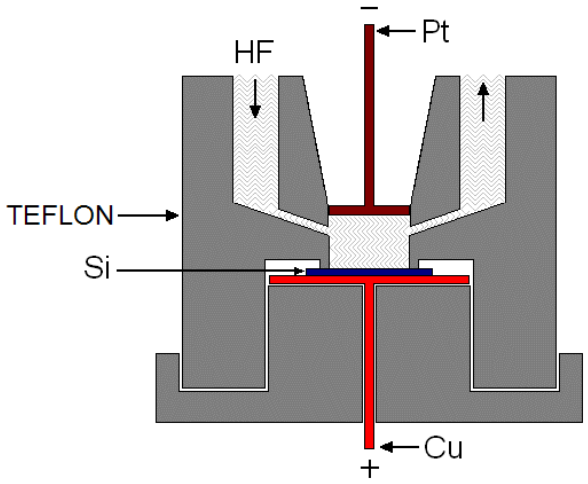

Figure 1. Schematic representation of the Teflon etching cell used in the synthesis of porous silicon samples.

To characterize PSi films, spectroscopic ellipsometry (SE) is perhaps the most ideal non-invasive technique for determining, at the same time, the thickness, composition, refraction index (n) and extinction coefficient (k) of the film. SE measures the change in light polarization upon reflection from the sample surface to obtain the ellipsometric parameters ψ and Δ [3]. Measurement of these parameters repeated for each wavelength across a spectral range of interest can determine n and k as functions of light wavelength, as well as the thickness and composition of the PSi layer through a computer model.

In materials science, theoretical models can be classified as empirical, semi-empirical or *ab initio*. The density functional theory (DFT) is indubitably the most popular *ab initio* method for studying the ground-state properties of semiconductors, since the correct ground-state electronic density can be obtained by self-consistently minimizing the total energy density functional [4]. In this article, we report an *ab initio* quantum mechanical investigation of the effects of oxygen atoms on the PSi structure and its complex refractive index. The theoretical results are compared with experimental data obtained from SE.

2. Experimental procedure

The PSi samples used in this study were fabricated by an anodic electrochemical dissolution of p^+-type (001)-oriented c-Si wafers with an electrical resistivity of 0.01–0.03 Ω cm in an aqueous 33% HF/67% ethanol electrolyte [5]. In order to ensure electrical conduction during the anodization, a gold film was deposited on the backside of the c-Si substrate. The etching cell that was used is illustrated schematically in figure 1, where a dc electrical current of 150 mA was applied between the platinum electrode and copper contact during 50 s, obtaining a PSi layer of thickness about 2.3 μm. The electrolyte was recycled by a mechanical pump in order to remove air bubbles generated by the electrochemical reaction and to improve the homogeneity of the PSi thin films. The porous-area diameter of the samples was approximately 1.5 cm. After etching, the samples, numbered 1–5, were rinsed with ethanol and thermally oxidized in an oxygen atmosphere at 150, 300, 450, 600, and 750 °C, respectively, for 15 min. The measurement of SE was carried out on a Jobin–Yvon UVISEL spectroscopic ellipsometer and

the data analysis was partially performed by means of DeltaPsi2 software provided by the same company.

3. Calculation method

It is well known that there is preferential growth of pores along the [001] crystallographic directions in p^+-type (001)-oriented c-Si wafers [6, 7]. For numerical calculations, we start from a supercell of 32 atoms built by joining four cubic c-Si cells of eight atoms on the x–y plane, and then square empty columns are dug along the z-direction by removing 13 centre Si atoms [8], which produces a weight porosity of about 40%. The surface dangling bonds are saturated by using hydrogen and oxygen atoms, in order to simulate different degrees of sample oxidation. This pore model based on supercells has the advantage of being simple and emphasizes the effects of quantum confinement and interconnection of the skeleton structure.

Once the pore model is chosen, the electronic behaviour is investigated in this work by an *ab initio* non-relativistic quantum mechanical analysis. In particular, the DFT calculations were carried out by using the local density approximation (LDA) and the nonlocal gradient-corrected exchange–correlation functional (GGA) for the self-consistent total energy calculation. Unfortunately, for semiconductors and insulators, both LDA and GGA underestimate the band gap by 30%–50% [9], which is usually corrected by rigidly shifting the conduction band to higher energies through a scissors operator (ΔE) [10]. In particular, for the case of silicon, $\Delta E = 0.6$ eV is selected [11]. This scissors operator could be omitted if a many-body GW [dressed Green's function (G) and dynamically screened Coulomb interaction (W)] and/or DFT + U approach is used [12]. However, such an approach requires much more computing time, especially combined with a supercell model.

All *ab initio* calculations in this study have been performed with the CASTEP codes developed at Cambridge University, UK [13], which is considered as one of the most precise DFT plane-wave pseudopotential programs. Specifically, the electronic wavefunctions are expanded in a plane-wave basis set truncated at a cutoff energy $E_c = 900$ eV due to the presence of hydrogen atoms [14]. To calculate the optical properties properly, norm-conserving pseudopotentials are used in which the scattering process is correctly reproduced by requiring the integrals of squared amplitudes of pseudo-and all-electron wavefunctions to be identical inside the core region [9]. The first Brillouin zone is represented by a **k**-point sampling with a constant spacing $\Delta k = 0.02$ Å^{-1}, where each point has a specific weight given by the Monkhorst and Pack method [15]. An ultra-fine self-consistent field tolerance of 5×10^{-7} eV/atom is used for both geometry optimization and optical property calculations.

4. Results

On the theoretical side, a full geometry optimization has been performed in the configuration space by means of the Broyden–Fletcher–Goldfarb–Shanno (BFGS) quasi-Newton minimization algorithm [16], which allows the atoms to find their minimal energy positions. The constraints used in this geometry optimization were three right angles of the supercells and its lengths along the x and y directions, allowing relaxation of the z-direction length (a_z), in order to simulate the fact that PSi samples are constrained by c-Si in the x–y plane. The pore surface is initially saturated by 20 hydrogen atoms, and during the oxidation process they are gradually substituted by oxygen atoms, leading to a maximum number of eight oxygen atoms without producing a significant structural distortion. In figure 2, the minimal energy structures from the z-direction view are illustrated for supercells containing from zero to eight oxygen atoms (small red spheres), where an oxygen–silicon ring is formed at the pore surface for the case of eight oxygen atoms. The a_z obtained from the LDA (solid dots) and

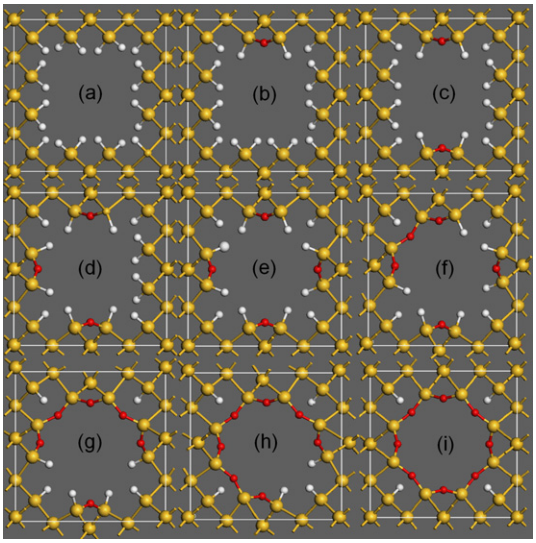

Figure 2. (a)–(i). Z-direction view of nine geometrically optimized supercells containing from zero to eight oxygen atoms (small red spheres) respectively, and hence from 20 to four hydrogen atoms (small white spheres) and 19 silicon atoms (yellow large spheres) each.

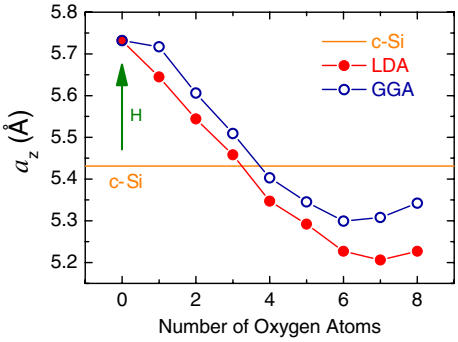

Figure 3. Z-direction supercell lattice parameter obtained from LDA (solid dots) and from GGA (open dots) versus the number of oxygen atoms in the supercell, compared with that of c-Si (solid line). The arrow indicates the lattice expansion when the pore surface is fully saturated by hydrogen atoms.

from the GGA (open dots) are shown comparatively in figure 3, in comparison with that for c-Si (solid line). Observe the structural contraction as the oxygen content grows, contrary to the hydrogen case, in which the porous structure expands due to the hydrogen–hydrogen interaction [14]. The contraction observed in the oxygen case could be related to the fact that the distance between the second-neighbour silicon atoms in SiO_2 quartz is much smaller than that in c-Si, being 3.057 and 3.840 Å, respectively. Hence, the presence of oxygen atoms on the pore surface produces a local diminution of the second-neighbour separations, and consequently a structural contraction.

The imaginary part of the dielectric function (ε) can be written as [17]

$$\mathrm{Im}[\varepsilon(\omega)] = \frac{2e^2\pi}{\Omega\varepsilon_0}\sum_{k,\mathrm{v},\mathrm{c}}\left|\left\langle\Psi_k^{\mathrm{c}}\right|\hat{e}\cdot\boldsymbol{r}\left|\Psi_k^{\mathrm{v}}\right\rangle\right|^2\delta\left(E_k^{\mathrm{c}}-E_k^{\mathrm{v}}-\hbar\omega\right), \tag{1}$$

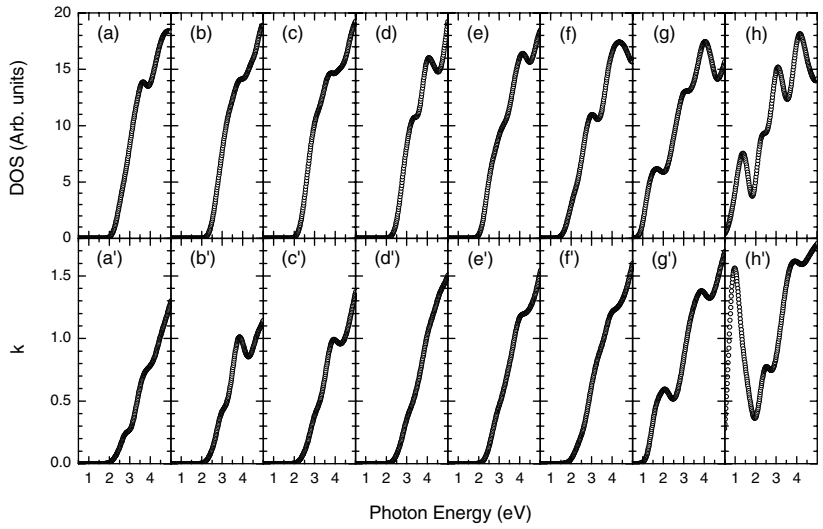

Figure 4. (a)–(h) Density of states (DOS) and (a′)–(h′) extinction coefficient (k) for structures shown in figures 2(b)–(i), respectively.

where $\hat{e}$ is the light-polarization unitary vector, Ω is the volume of supercell, E_k^{v} and E_k^{c} are energies associated with the wavefunctions Ψ_k^{v} and Ψ_k^{c} respectively, where the superscript indexes v and c correspondingly stand for the valence and conduction bands. The real part of the dielectric function is linked to Im[ε] by the Kramers–Kronig transformation. For non-magnetic materials, the complex refractive index, $N = n - \mathrm{i}k$, can be calculated through $\mathrm{Re}[\varepsilon] = n^2 - k^2$ and $\mathrm{Im}[\varepsilon] = -2nk$. It is worth mentioning that a smearing width of 0.2 eV, leading to a Gaussian broadening of the dielectric function, is introduced to include thermal, structural, and/or chemical impurity effects. The optical property calculations are performed within the LDA scheme, since it gives the correct sum rule for the exchange–correlation hole [18]. In figure 4, the density of states (DOS) and the extinction coefficient (k) corresponding to the structures illustrated in figures 2(b)–(i) are plotted, where the zero in the DOS spectra refers the top of the valence band. Notice the formation of an impurity state in the band gap when the oxygen content grows, which seems to be related to the oxygen–silicon ring located at the surface of the pore, as seen in figure 2(i).

On the other hand, the optical properties of the PSi samples are characterized by means of SE, where the ellipsometric data were acquired at an angle of incidence of 70° in the range 1.5–5.5 eV with a step of 0.01 eV. In figure 5, the SE variables I_{s} and I_{c} as a function of photon energy are plotted for samples 1–5 with different thermal oxidation temperatures, indicated in the figures. Let us observe that there is an oscillating behaviour below 3 eV, since the PSi film is almost transparent, and for higher photon energies it becomes very absorbent. Also, the band gap of PSi film, indicated by the highest energy of the oscillating region, increases slightly with oxygen content.

Let us consider a four-layer model to simulate a PSi film, in which uniform layers are placed over a substrate of c-Si and each layer is supposed to be composed of three materials: c-Si, air, and SiO_2. Starting from the known dielectric functions of these three components, I_{s} and I_{c} spectra can be fitted by means of the Bruggeman effective medium approximation [19], adjusting the layer thickness and the percentage of each component. This fitting procedure was performed in the oscillating region of the I_{s} and I_{c} spectra by using the DeltaPsi2 software,

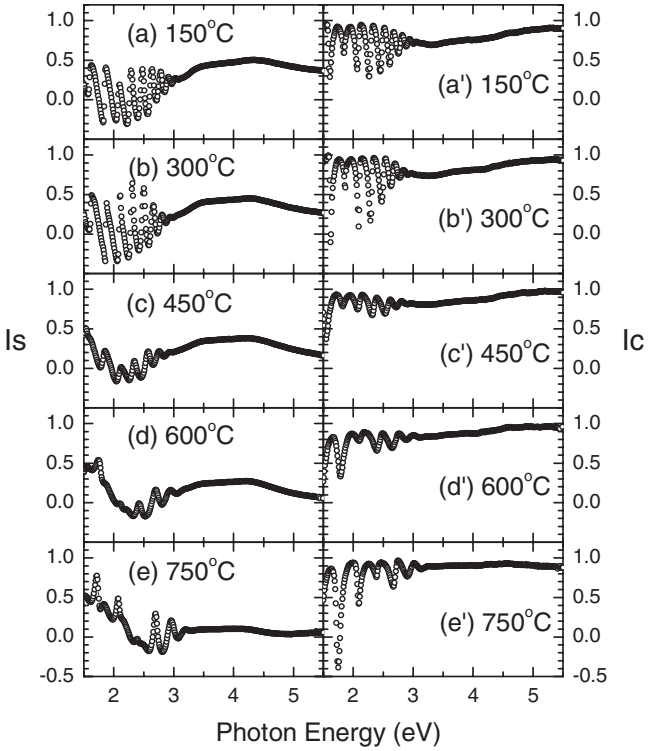

Figure 5. Ellipsometric variables (a)–(e) I_s and (a′)–(e′) I_c as a function of photon energy for samples 1–5, respectively. The thermal oxidation temperature of the sample is indicated in each figure.

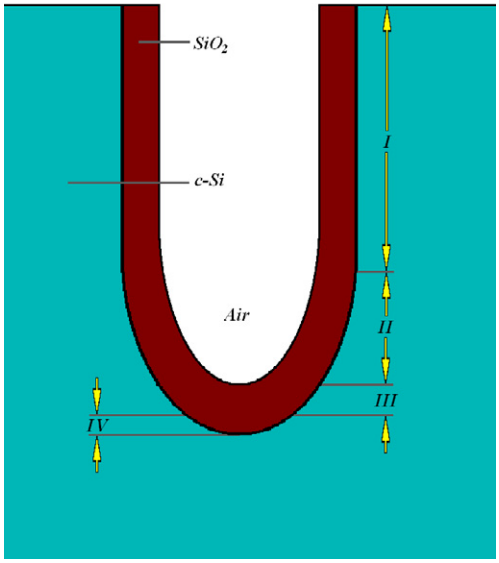

Figure 6. Schematic illustration of a pore in the PSi film after thermal oxidation.

Table 1. Thickness and composition obtained by using a four-layer model.

Thickness (nm) [c-Si/air/SiO_2 (%)]	Sample 1	Sample 2	Sample 3	Sample 4	Sample 5
Layer I	1412 [21/79/0]	1395 [22/78/0]	1870 [7/41/52]	1175 [0/51/49]	1186 [0/53/47]
Layer II	970 [17/59/24]	926 [17/55/28]	335 [4/22/74]	860 [0/26/74]	921 [0/40/60]
Layer III	75 [22/1/77]	74 [24/1/75]	66 [25/1/74]	63 [23/0/77]	62 [21/0/79]
Layer IV	46 [54/0/46]	44 [55/0/45]	38 [64/0/36]	32 [64/0/36]	33 [62/2/36]

and the results are shown in table 1. Notice that all the samples have a PSi-film thickness of between 2100 and 2600 nm, which has been confirmed by optical microscopy. The porosity of these samples, revealed by this four-layer model, decreases with thermal oxidation, which could be due to the formation of a SiO_2 skin on the pore surface, as shown schematically in figure 6. The thickness and composition of layers III and IV seem to confirm this hypothesis.

From the I_s and I_c spectra, where $I_s = \sin(2\psi)\sin(\Delta)$ and $I_c = \sin(2\psi)\cos(\Delta)$ [20], the complex refractive index ($N_1 = n - ik$) of the PSi film can be determined by using equations of reflection ellipsometry for ambient(0)–film (1)–substrate (2) systems [3],

$$\tan(\psi)e^{i\Delta} = \rho = \frac{r_{0,1p} + r_{1,2p}e^{-i2\beta}}{1 + r_{0,1p}r_{1,2p}e^{-i2\beta}} \times \frac{1 + r_{0,1s}r_{1,2s}e^{-i2\beta}}{r_{0,1s} + r_{1,2s}e^{-i2\beta}}, \tag{2}$$

where $\beta = 2\pi N_1 \cos(\phi_1) d_1/\lambda$ is the phase angle, with d_1 being the thickness of the film and λ being the light wavelength, and the coefficients of Fresnel reflection for the s- and p-polarization lights are given by

$$r_{m,m+1s} = \frac{N_m \cos(\phi_m) - N_{m+1}\cos(\phi_{m+1})}{N_m \cos(\phi_m) + N_{m+1}\cos(\phi_{m+1})} \tag{3}$$

and

$$r_{m,m+1p} = \frac{N_{m+1} \cos(\phi_m) - N_m \cos(\phi_{m+1})}{N_{m+1} \cos(\phi_m) + N_m \cos(\phi_{m+1})}, \tag{4}$$

with m being the index of the medium, 0 or 1. Additionally, the complex refractive indices (N_m) of these three media are related by Snell's law [3]:

$$N_0 \sin(\phi_0) = N_1 \sin(\phi_1) = N_2 \sin(\phi_2). \tag{5}$$

Therefore, for given N_0, N_2, d_1, λ, and ϕ_0, n and k of the PSi film can be calculated by using equations (2)–(5) and the spectra of I_s and I_c. This calculation has been perfomrmed and the results are shown in figure 7, where a multi-solution picture is found because equations (2)–(5) are nonlinear. However, k has a unique physical solution that is different from zero for photon energies larger than 3 eV, which leads to an answer of n being mainly less than unity in the same region of energy. By applying the condition of continuity to the complex refractive index as a function of photon energy, the n and k spectra could be determined. Observe that the magnitude of k decreases with thermal oxidation. This fact is in agreement with the results of the four-layer model shown in table 1, since the thermal oxidation diminishes the c-Si content, which is mainly responsible for photon absorption in this range of energies within the Bruggeman effective medium approximation.

5. Conclusions

In this work, we have performed an *ab initio* quantum mechanical study of the effects of oxygen atoms on the PSi structure and its optical properties. To our knowledge, this is the first *ab*

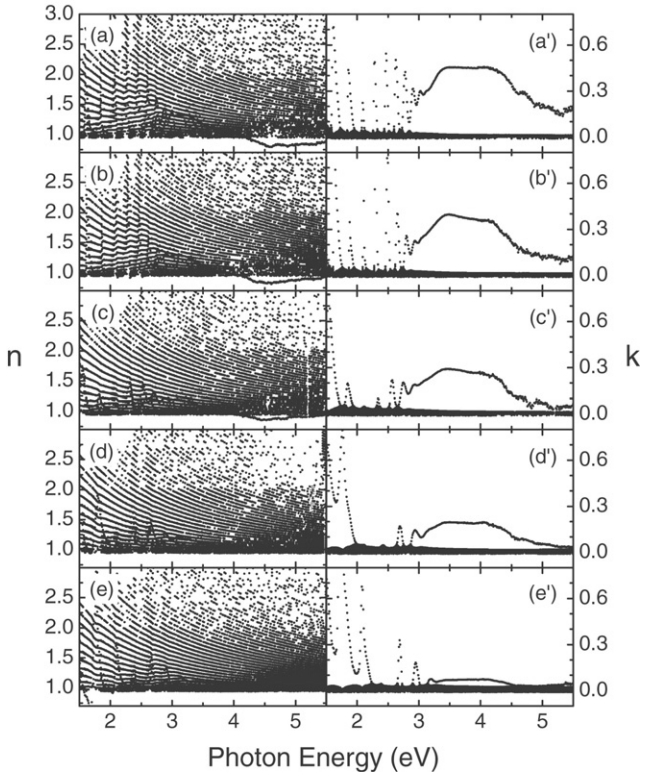

Figure 7. (a)–(e) Refraction index (n) and (a′)–(e′) extinction coefficient (k) of PSi films, obtained from the I_s and I_c spectra of figure 5, corresponding to samples 1–5, respectively.

initio study of the oxidation process in PSi by using an interconnected supercell structure. This supercell model leads to folding of the Brillouin zone [21] and then the minimum of the c-Si conduction band shifts towards the centre of the Brillouin zone, i.e. the band gap becomes direct. This artificial folding becomes real when empty-column pores are dug, i.e. the supercell transforms into the unit cell of the system. At the same time, the presence of empty columns introduces extra nodes in the wavefunctions, which leads to a quasi-confinement effect on the band structure through a broadening of the band gap; even the wave functions are still extended [8, 14]. The combination of these two effects, folding plus quasi-confinement, produces a band gap of about 2.5 eV for the structure analysed in this article. Moreover, both LDA and GGA results show a contraction of the PSi structure due to the presence of oxygen atoms, contrary to the expansion observed when the pore surface is fully saturated by hydrogen atoms [14].

Simultaneously, we have synthesized PSi thin films through etching p-type c-Si in hydrofluoric acid solution. The measurement of its optical properties was carried out by means of spectroscopic ellipsometry, which provides a rich source of information and is sometimes difficult to extract. That is the case for a complex refractive index of PSi film, where we have developed new software to determine the physical solution of n and k of the film, since the ellipsometer company does not provide this. Finally, the difference observed between the theoretical and experimental spectra of k, i.e. a band gap of 2.5 eV versus 3 eV as well as a maximum k value of 1.5 versus 0.5, could be understood, since the theoretical sample porosity

is smaller than the experimental porosity, being about 40% versus 60%. It is important to stress that the porosity has a deep effect on the quantum-confinement strength, as well as on the absorption capability.

Acknowledgments

We gratefully acknowledge discussions with Octavio Gómez, Sandra Rodil, and Aurelian C Galca. The technical assistance of Silvia E Frausto is also fully appreciated. This work has been partially supported by UNAM-IN110305 and CONACyT-58938. Computations were performed at Bakliz and Kanbalam of Dirección General de Servicios de Cómputo Académico, Universidad Nacional Autónoma de México.

References

[1] Poole C P and Owens F J 2003 *Introduction to Nanotechnology* (New York: Wiley)
[2] Canham L T (ed) 1999 *Properties of Porous Silicon* (London: INSPEC)
[3] Azzam R M A and Bashara N M 1987 *Ellipsometry and Polarized Light* (Amsterdam: North-Holland/Elsevier Science)
[4] Hohenberg P and Kohn W 1964 *Phys. Rev.* **136** B864
[5] Nava R, Agarwal V, del Rio J A and Wang C 2003 *J. Non-Cryst. Solids* **329** 140
[6] Cullis A G, Canham L T and Calcott P D J 1997 *J. Appl. Phys.* **82** 909
[7] Christophersen M, Carstensen J, Rönnebeck S, Jäger C, Jäger W and Föll H 2001 *J. Electrochem. Soc.* **148** E267
[8] Cruz M, Wang C, Beltrán M R and Tagüeña-Martínez J 1996 *Phys. Rev.* B **53** 3827
[9] Payne M C, Teter M P, Allan D C, Arias T A and Joannopoulos J D 1992 *Rev. Mod. Phys.* **64** 1045
[10] Del Sole R and Girlanda R 1993 *Phys. Rev.* B **48** 11789
[11] Bonder Y and Wang C 2006 *J. Appl. Phys.* **100** 044319
[12] Miyake T, Zhang P, Cohen M L and Louie S G 2006 *Phys. Rev.* B **74** 245213
[13] Segall M D, Lindan P J D, Probert M J, Pickard C J, Hasnip P J, Clark S J and Payne M C 2002 *J. Phys.: Condens. Matter* **14** 2717 see also the detailed help of Materials Studio Modeling 4.0 (Accelrys, 2006)
[14] Vázquez E, Tagüeña-Martínez J, Sansores L E and Wang C 2002 *J. Appl. Phys.* **91** 3085
[15] Monkhorst H J and Pack J D 1976 *Phys. Rev.* B **13** 5188
[16] Press W H, Teukolsky S A, Vetterling W T and Flannery B P 1992 *Numerical Recipes* 2nd edn (New York: Cambridge University Press)
[17] Cruz M, Beltrán M R, Wang C, Tagüeña-Martínez J and Rubo Y G 1999 *Phys. Rev.* B **59** 15381
[18] Harris J and Jones R O 1974 *J. Phys. F: Met. Phys.* **4** 1170
[19] Tompkins H G and McGahan W A 1999 *Spectroscopic Ellipsometry and Reflectometry, a User's Guide* (New York: Wiley)
[20] Gaillet M, Guendouz M, Ben Salah M, Le Jeune B and Le Brun G 2004 *Thin Solid Films* **455** 410
[21] Altmann S L 1991 *Band Theory of Solids: an Introduction from the Point of View of Symmetry* (New York: Oxford University Press) p 147